Calculation of Timing and Amplitude Jitter in Dispersion-Managed Optical Fiber Communications Using Linearization

V. S. Grigoryan, C. R. Menyuk, and R.-M. Mu

Abstract—An approach based on linearization that allows us to calculate the timing and amplitude jitter for arbitrary pulse shapes in dispersion-managed fibers is developed. We apply this approach to calculate the jitter for dispersion-managed soliton, return-to-zero (RZ), and nonreturn-to-zero (NRZ) transmission formats. We then estimate the bit error rates. The approach described here yields more precise results than Monte Carlo simulations at a fraction of the computational cost.

Index Terms— Dispersion management, noise, jitter, optical fiber transmission.

I. INTRODUCTION

AMPLIFIED spontaneous emission (ASE) noise and interchannel interference cause fluctuations of the time and energy of signal pulses. The temporal fluctuations are referred to as timing jitter, while the pulse energy fluctuations are referred to as amplitude jitter. These fluctuations degrade the phase and amplitude margins, respectively, leading to errors. Fundamental parameters determining the timing and amplitude jitter are the variance of the pulse's central time and the variance and average of the pulse energy. The time variance was calculated for the first time by Gordon and Haus [1], [2] for a hyperbolic secant soliton pulse propagating in a fiber with uniform dispersion. One of the key ideas used in [1] and [2] was linearization of the problem about the analytically known soliton solution. The linearization was feasible because the noise power is much weaker than the signal power. In dispersion-managed fibers one cannot directly apply the Gordon–Haus theory in most cases because the pulse shapes may differ significantly from the analytically assumed hyperbolic-secant shape. For dispersion-managed solitons, the pulse shapes range from hyperbolic-secant to Gaussian to flat-top, depending on the strength of the dispersion management [3], [4], and oscillate periodically. For return-to-zero (RZ) and nonreturn-to-zero (NRZ) signals, the pulse shapes differ even more from the hyperbolic secant shape and evolve continually.

For dispersion-managed solitons, it was predicted in [3] that a corrected Gordon–Haus formula reduced by the enhancement factor (the ratio of the dispersion-managed soliton energy to the energy of a standard soliton in fibers with equal path-average dispersion) would successfully describe

The authors are with the Department of Computer Science and Electrical Engineering, University of Maryland, Baltimore County, Baltimore, MD 21228 USA (e-mail: grigorya@umbc.edu).

the timing jitter. This prediction is roughly correct [4], but it is intuitively clear that the timing jitter must be sensitive to pulse bandwidth—the greater the bandwidth of the pulse, the greater the amount of noise the pulse can incorporate. Different pulse shapes have different bandwidths. Hence, the Gordon–Haus formula reduced by the enhancement factor will not yield exactly accurate results. Recently, a new approach was suggested [5]–[7] that takes into account the more general dispersion-managed soliton (DMS) pulse shape. However, this work still presumes an analytically fixed pulse shape with quadratic chirp that can change only its duration and amplitude. This approach yields only a rough approximation of the jitter for solitons and cannot describe the jitter at all for RZ and NRZ signals. Another approach that has been used for NRZ signals is to linearize the noise around an assumed continuous wave signal to calculate the noise power [8]–[11]. This approach is fairly successful when the pulse evolution is not too large, but it cannot determine the effect of timing jitter. Direct Monte Carlo simulations can be used to fill this gap, but processing the large number of different realizations of random noise that is required to obtain an accurate solution can be very numerically time-consuming. Thus, developing a general approach that allows us, first, to calculate the timing and amplitude jitter for arbitrary pulse shapes and, second, to avoid time-consuming Monte Carlo simulations, is vitally important.

We stress that the linearization approach, used in the Gordon–Haus theory [1], [2], has a much broader range of applicability in optical fiber communications than just for hyperbolic-secant solitons in uniform dispersion fibers, continuous wave signals [8]–[11], or other analytically known pulse shapes. The basic idea of the present paper is to use the linearization approximation around an arbitrary, numerically-determined solution of the nonlinear Schrödinger equation. In effect, we break the problem into two steps. In the first, we determine the signal evolution in the absence of noise. While this step requires computational methods for arbitrary pulse shapes, it is fully deterministic and thus does not require the use of many realizations. In the second step, we linearize around the numerically determined solution, using statistical properties of the ASE noise to derive dynamic equations for the mean and variance of a pulse's central time and energy. We show that in the limits of the linearization approximation the pulse's central time is Gaussian-distributed with the variance and average calculated by our method. The situation with the amplitude jitter is a bit more complex. In order for the linearization approximation to be valid, the

spontaneous-spontaneous beat noise of a single noise mode must be small compared to the signal–spontaneous beat noise. However, the number of noise modes is approximately equal to $B_{opt}T_w$, where B_{opt} is the optical bandwidth and T_w is the bit window. When this number becomes large, it is not possible to neglect the spontaneous–spontaneous beat noise even when the linearization approximation is valid. When the number of noise modes is small, so that sum of the spontaneous-spontaneous beat noise contributions from all the noise modes can be ignored, the signal's central energy is Gaussian-distributed with the variance and average calculated by our method. When the number of noise modes is large, and the amount of energy that goes into each noise mode is the same, the signal energy is Rician-distributed [8], [9], [12]. More generally, the energy is chi-square-distributed [12]. In typical cases that we considered, the variance of the noise energy is about 1/100 of the signal energy, while $B_{opt}T_w \lesssim 10$, so that it is reasonable to ignore spontaneous-spontaneous beat noise which is what we do in this paper. When either timing jitter or amplitude jitter becomes the dominant source of errors, it is then possible to calculate the bit error rate which we show how to do. We compare our theoretical approach to simulations for a wide range of pulse formats, including DMS, RZ, and NRZ pulses.

The remainder of this paper is organized as follows. In Section II, we derive the basic equations for the variance of the central time and energy of the pulse in the presence of ASE noise. In Section III, we validate our approach by comparing the timing and amplitude jitter predicted by theory to the results of Monte Carlo simulations over a large number of realizations of the ASE noise. In Section IV, we show how we estimate the bit error rate probability knowing the variances of the central time and the energy of the signal pulses.

II. BASIC EQUATIONS

We start from the nonlinear Schrödinger equation written in Langevin form

$$i\frac{\partial u}{\partial z} + \frac{1}{2}[D(z) - ib(z)]\frac{\partial^2 u}{\partial t^2} + C|u|^2 u = ig(z)u + \hat{F}(z,t) \quad (1)$$

using a formulation due to Haus [2] that is particularly useful for noise problems. In this formulation $|u|^2$ is the photon flow, t is unnormalized time, $z = |\beta_0''|Z$ is the product of a scaling dispersion β_0'' and the unnormalized distance Z, while $D(z)$ and $b(z)$ are the local dispersion and filtering normalized with respect to $|\beta_0''|$. The quantity $C = n_2\hbar\omega^2/cA_{eff}|\beta_0''|$ is the nonlinear coefficient, where n_2 is the Kerr coefficient, ω is the signal's central frequency, A_{eff} is the effective fiber cross section, and c is the speed of light. The gain $g(z)$ may be written

$$g(z) = \begin{cases} g_0, & z_n < z < z_n + L_{amp} \\ -\Gamma, & \text{elsewhere} \end{cases}$$

where g_0 and Γ are respectively the gain and loss coefficients in the optical fiber, z_n is the position of the n-th amplifier, and L_{amp} is the amplifier length. The noise contribution $\hat{F}$ from the amplifiers has the autocorrelation function

$$\langle\hat{F}(z,t)\hat{F}^*(z',t')\rangle = 2g_0\theta(z)\delta(z-z')\delta(t-t') \quad (2)$$

where $\theta(z)$ is the spontaneous emission factor n_{sp} when $z_n < z < z_n + L_{amp}$, and we set $\theta(z) = 0$ elsewhere since there is no noise contribution outside the amplifiers. We also define the central pulse time t_p, central frequency Ω, and photon number U in the pulse as

$$t_p = \int_{-\infty}^{\infty} t|u|^2\,dt/U, \quad \Omega = \int_{-\infty}^{\infty}(u_t u^* - u_t^* u)\,dt/2iU,$$

$$U = \int_{-\infty}^{\infty}|u|^2\,dt \quad (3)$$

where the subscript t designates the partial time derivative, so that $u_t \equiv \partial u/\partial t$.

A. Timing Jitter and Unfiltered System

Differentiating t_p, Ω, and U in (3) with respect to z and combining them with (1) where $b(z) = 0$ we derive the following dynamic equations for the central time t_p and central frequency Ω of a signal pulse,

$$\frac{dt_p}{dz} = D\Omega + \frac{i}{U}\int_{-\infty}^{\infty}(t - t_p)(u\hat{F}^* - u^*\hat{F})\,dt$$

$$\frac{d\Omega}{dz} = i\frac{\Omega}{U}\int_{-\infty}^{\infty}(u^*\hat{F} - u\hat{F}^*)\,dt + \frac{1}{U}\int_{-\infty}^{\infty}(u_t^*\hat{F} + u_t\hat{F}^*)\,dt. \quad (4)$$

Implicit solutions of (4) are

$$t_p = \mathcal{F} + \mathcal{S} \quad (5)$$

where

$$\mathcal{F} = \int_0^z D\Omega\,dz',$$

$$\mathcal{S} = i\int_0^z \left\{\frac{1}{U}\int_{-\infty}^{\infty}(t - t_p)[q^*\hat{F}\exp(-i\Omega t) - q\hat{F}^*\exp(i\Omega t)]\,dt\right\}dz'$$

$$\Omega = \Omega_0 + \int_0^z \left\{\frac{1}{U}\int_{-\infty}^{\infty}[q_t^*\hat{F}\exp(-i\Omega t) + q_t\hat{F}^*\exp(i\Omega t)]\,dt\right\}dz \quad (6)$$

$q = u\exp(-i\Omega t)$ is a new field shifted such that its central frequency is zero, and Ω_0 is the central frequency of the input pulse. As is seen from (5) the time position deviation is a superposition of the time shift $\mathcal{F}$ induced by the frequency shift and the time shift $\mathcal{S}$ due to the direct impact of the noise on the pulse. We represent the solution of (1) as $u = \bar{u} + \delta u$ where δu is a small noise contribution such that second- and higher order corrections to $\mathcal{F}, \mathcal{S}$, and Ω are negligible. Since $\delta u \propto \hat{F}$, it follows that one can neglect the contribution of δu to the right-hand sides of (6). Using (2), (5), and (6), we can calculate the variance of the central pulse time t_p

$$\sigma_t^2 = \langle t_p^2\rangle - \langle t_p\rangle^2 = A + B + C \quad (7)$$

where, defining a scalar product

$$(\delta q_i, \delta q_j) = \int_{-\infty}^{\infty}(\delta q_i\delta q_j^* + \delta q_i^*\delta q_j)\,dt \quad (8)$$

and the components

$$\delta q_1 = 2\sqrt{g_0}\theta q_t/U,$$
$$\delta q_2 = 2i\sqrt{g_0}\theta(t - t_p)q/U \qquad (9)$$

we find that

$$A = \langle \mathcal{F}^2 \rangle = \int_0^z D(z_1)\,dz_1$$
$$\cdot \int_0^{z_1} D(z_2)\,dz_2 \int_0^{z_2} (\delta q_1, \delta q_1)\,dz_2',$$
$$B = 2\langle \mathcal{F}\mathcal{S} \rangle = \int_0^z D(z_1)\,dz_2 \int_0^{z_1} (\delta q_1, \delta q_2)\,dz_1'$$
$$C = \langle \mathcal{S}^2 \rangle = \frac{1}{2}\int_0^z (\delta q_2, \delta q_2)\,dz'. \qquad (10)$$

Equations (7) and (10) have a simple physical interpretation. We note that one can always expand the noise in a series of orthogonal functions such that

$$\hat{F}(z,t)\exp(-i\Omega t) = \delta q_1(z,t) + \overline{\delta q_2}(z,t) + \delta q_r(z,t) \qquad (11)$$

where $\overline{\delta q_2} = a\delta q_1 + \delta q_2$ is made orthogonal to δq_1 by setting $a = -(\delta q_1, \delta q_2)/(\delta q_1, \delta q_1)$ and δq_r is a remainder that is orthogonal to both δq_1 and $\overline{\delta q_2}$. In this case, substituting (11) into right-hand side of (6) one can see that δq_1 generalizes what Gordon and Haus [1] refer to as the noise field phasor component that shifts the central frequency Ω. Similarly, δq_2 generalizes the component of the noise field that directly shifts the time. We note that no reference to inverse scattering theory or soliton perturbation theory is required to obtain either noise component. All the functions on the right-hand sides of (10), q, U, t_p, and Ω, are determined by the unperturbed solution $\bar{u}$ of (1) with no noise contribution. From the equation for Ω in (6) we also find that the variance of the frequency in one amplifier is

$$\langle \delta\Omega^2 \rangle = [(G-1)/(2g_0)](\delta q_1, \delta q_1)$$
$$= 2\theta(G-1)\int_{-\infty}^{\infty} |q_t|^2\,dt/U^2 \qquad (12)$$

where $G = \exp(2g_0 L_{\text{amp}})$ is the total amplifier gain and L_{amp} is the amplifier length. Equations (10) and (12) are valid for any arbitrary pulse shape and represent a key result of the paper. Integrals on the right-hand sides of (10) can easily be calculated numerically once $\bar{u}$ is known computationally. Although (7)–(10) appear complex at first sight, they have a simple physical meaning. The terms A, B, and C are responsible for the timing jitter due to the frequency shift, timing jitter due to the pulse chirp, and the timing jitter due to direct time offset. Equations (7)–(10) and (12) differ from the Gordon–Haus theory [1], [2] in two respects. First, the variance of the frequency shift after an amplifier is proportional to the ratio of the square of the pulse bandwidth divided by the pulse energy. This result is physically intuitive because when the bandwidth of a pulse becomes larger, the pulse will incorporate a larger amount of the noise radiation. On the other hand, when the pulse energy becomes larger, then the influence of the incorporated noise becomes smaller. This frequency shift translates into a shift of the central time which is the contribution of the A term. Second, the B term

represents a contribution to the timing jitter caused by the pulse chirp. This term contains a new physical effect that is not in the Gordon–Haus calculation because standard solitons are unchirped. To understand this effect, we recall that there exist two sources of the time shift. The first is the frequency shift, represented by the term $\mathcal{F}$ in (5), and the second is the time offset, represented by the term $\mathcal{S}$ in (5). Consequently, the term A represents the timing jitter induced by the frequency shift alone, the term C represents the timing jitter induced by the direct time offset alone. The term B represents the interference between the two effects. Physically, the B term has the following origin. If a pulse has a chirp, then its local frequency depends on time, so that a time offset leads to a frequency shift that in its turn translates into an additional shift in the pulse's central time. The interference term B can either increase or decrease the total timing jitter depending on the sign of the chirp. For example, if we consider a chirped pulse $q = |q|\exp[i\alpha(t - t_p)^2]$, then the scalar cross product becomes

$$(\delta q_1, \delta q_2) = 16\alpha\frac{g_0\theta}{U^2}\int_{-\infty}^{\infty}(t - t_p)^2|q|^2\,dt. \qquad (13)$$

Hence, it follows from (10) that when the product $D\alpha$ is positive then B is positive, increasing the jitter; however, if the product $D\alpha$ is negative then the opposite occurs.

B. Timing Jitter Filtered System

As in the previous section, we differentiate t_p, Ω, and U in (3) with respect to z and combine them with (1) to derive dynamic equations for the central time t_p and central frequency Ω of a signal pulse. In this case, $b(z) \neq 0$ which allows us to include filtering. We note that only quadratic filters are included in (1), but our results can be generalized without much difficulty to include more general filters. We now obtain

$$\frac{dt_p}{dz} = D\Omega + \frac{i}{U}\int_{-\infty}^{\infty}(t - t_p)[ib|q_t|^2$$
$$- b\Omega(qq_t^* - q^*q_t) + \hat{F}_1]\,dt,$$
$$\frac{d\Omega}{dz} = \frac{1}{U}\int_{-\infty}^{\infty}\left\{-b\left[2\Omega|q_t|^2 + \frac{i}{2}(q_tq_{tt}^* - q_t^*q_{tt})\right] + \hat{F}_2\right\}dt \qquad (14)$$

where

$$\hat{F}_1 = q\exp(i\Omega t)\hat{F}^* - q^*\exp(-i\Omega t)\hat{F}$$
$$\hat{F}_2 = q_t^*\exp(-i\Omega t)\hat{F} + q_t\exp(i\Omega t)\hat{F}^*. \qquad (15)$$

Implicit solutions of (14) are again

$$t_p = \mathcal{F} + \mathcal{S} \qquad (16)$$

where

$$\mathcal{F} = \int_0^z \hat{D}\Omega\,dz'$$
$$\mathcal{S} = -\int_0^z \left\{\frac{1}{U}\int_{-\infty}^{\infty}(t - t_p)[b|q_t|^2 + i\hat{F}_1]\,dt\right\}dz' \qquad (17)$$

and

$$\hat{D} = \left[D - \frac{ib}{U} \int_{-\infty}^{\infty} (t - t_p)(qq_t^* - q^* q_t) \, dt \right] B_f \tag{18}$$

$$\Omega = \Omega_0 + \int_0^z \left\{ \frac{1}{2U} \int_{-\infty}^{\infty} [ib(q_t^* q_{tt} - q_t q_{tt}^*) + 2\hat{F}_2] \, dt \right\} dz' \tag{19}$$

$$B_f = \exp\left[-2 \int_0^z b(z') \Omega_B^2(z') \, dz' \right] \tag{20}$$

$$\Omega_B^2 = \frac{1}{U} \int_{-\infty}^{\infty} |q_t|^2 \, dt. \tag{21}$$

Typically the filtering term is much smaller than the dispersion term. Substituting (18)–(21) into (17) and then (17) into (16), linearizing (16) around the unperturbed solution of (1), taking the square of (16), and using (2) and (8), we find the variance of the central time,

$$\sigma_t^2 = \langle t_p^2 \rangle - \langle t_p \rangle^2 = A + B + C \tag{22}$$

where now A, B, and C are

$$A = \langle \mathcal{F}^2 \rangle = \int_0^z \hat{D}(z_1) \, dz_1 \int_0^{z_1} \hat{D}(z_2) \, dz_2 \int_0^{z_2} (\delta\hat{q}_1, \delta\hat{q}_1) \, dz_2'$$

$$B = 2\langle \mathcal{FS} \rangle = \int_0^z \hat{D}(z_1) \, dz_2 \int_0^{z_1} (\delta\hat{q}_1, \delta q_2) \, dz_1' \tag{23}$$

$$C = \langle \mathcal{S}^2 \rangle = \frac{1}{2} \int_0^z (\delta q_2, \delta q_2) \, dz'$$

and where

$$\delta\hat{q}_1 = \frac{2\sqrt{g_0 \theta}}{U B_f} q_t. \tag{24}$$

We note that all the functions on the right hand sides of (22) and (23) are deterministic.

C. Amplitude Jitter

Differentiating U in (3) with respect to z and combining it with (1) we obtain

$$\frac{dU}{dz} = (2g - b\Delta^2)U + i \int_{-\infty}^{\infty} (u\hat{F}^* - u^*\hat{F}) \, dt \tag{25}$$

where we define the mean square central frequency of the pulse $\Delta^2 = \int_{-\infty}^{\infty} |u_t|^2 \, dt / U$. An implicit solution of (25) is

$$U = \left(U_0 + i \int_0^z \frac{1}{\mathcal{G}(z')} \left[\int_{-\infty}^{\infty} (u\hat{F}^* - u^*\hat{F}) \, dt \right] dz' \right) \mathcal{G}(z) \tag{26}$$

where U_0 is the input photon number of the pulse, and

$$\mathcal{G}(z) = \exp\left\{ \int_0^z (2g - b\Delta^2) \, dz' \right\} \tag{27}$$

represents the mean gain. Linearizing (26) and averaging the square of (26) using (2), we obtain the variance of the photon number in the signal pulse

$$\sigma_U^2 = \langle U^2 \rangle - \langle U \rangle^2 = 4U_0 g_0 \mathcal{G}^2(z) \int_0^z \frac{\theta(z')}{\mathcal{G}(z')} \, dz'. \tag{28}$$

It will be useful to define a normalized energy variance $\rho^2 = \sigma_U^2 / \langle U \rangle^2 = \sigma_U^2 / U_0^2 \mathcal{G}^2(z)$. In a system with periodically

distributed lumped amplifiers, in which $\mathcal{G} = 0$ after each amplifier, (28) reduces to

$$\rho^2 = \frac{\sigma_U^2}{\langle U \rangle^2} = 2n_{\text{sp}} \frac{G - 1}{U_0} K \tag{29}$$

where K is number of the amplifiers. Equation (29) implies that the increase of the normalized energy variance is proportional to the number of the noise photons per mode $n_{\text{sp}}(G - 1)K$ added to the pulse by K amplifiers. We note that due to filter losses $b\Delta^2$ in (25) the amplifier gain G in the filtered system must be higher compared to an unfiltered system to compensate for the extra loss in the filter. Consequently, the growth rate of the amplitude jitter is larger in a filtered system than in an unfiltered system.

III. COMPARISON WITH MONTE CARLO SIMULATIONS

To validate the use of linearization to calculate the timing and amplitude jitter, we simulated the propagation of signal pulses with different signal formats—RZ, NRZ, and DMS—in a dispersion-managed fiber with alternating spans of normal dispersion D_1 of length L_1 and anomalous dispersion D_2 of length L_2. We used the split-step method to solve (1) along with the Monte Carlo method to generate the ASE noise. We repeated the same calculations for a hundred different realizations of the ASE noise, except where stated, and collected their statistics to find the variance and the average of the pulse's central time and energy at the midpoint of anomalous dispersion span for each set of the system parameters. The loss coefficient of the fiber was 0.21 dB/km.

A. Dispersion-Managed Solitons

For DMS calculations we propagated single pulses. Fig. 1 compares the timing jitter calculated using Monte-Carlo simulations to the results of our linearization approach for DMS pulses with a pulse duration $t_{\text{FWHM}} = 20$ ps at the midpoint of the anomalous span. For a given average dispersion, the energy of the dispersion-managed solitons is larger than that of standard solitons, and this increase in energy is referred to as the enhancement factor. A simple theoretical approach to calculating the timing jitter is to use the Gordon-Haus formula for the timing jitter and to reduce it by the square root of the enhancement factor [3]. One can see in Fig. 1 that if the profile of the dispersion-managed soliton is nearly Gaussian, the difference between the reduced Gordon–Haus formula [3] and the Monte Carlo simulations, though visible at 10 Mm, remains small. In the case of Fig. 1(a) the energy enhancement factor is as large as 2.17. However, for more strongly dispersion-managed fibers with an energy enhancement factor of 8.16, shown in Fig. 1(b), the shape of the dispersion-managed soliton becomes more like a flat-top and its time-bandwidth product becomes larger, $\Delta\nu\Delta t = 0.661$ as compared to $\Delta\nu\Delta t = 0.424$ for a Gaussian. As the pulse bandwidth increases for a fixed pulse duration, the frequency shift increases in accordance with (12). The larger frequency shift translates into a larger contribution to the term A which at long distances makes the largest contribution to the timing jitter. The Gordon–Haus theory,
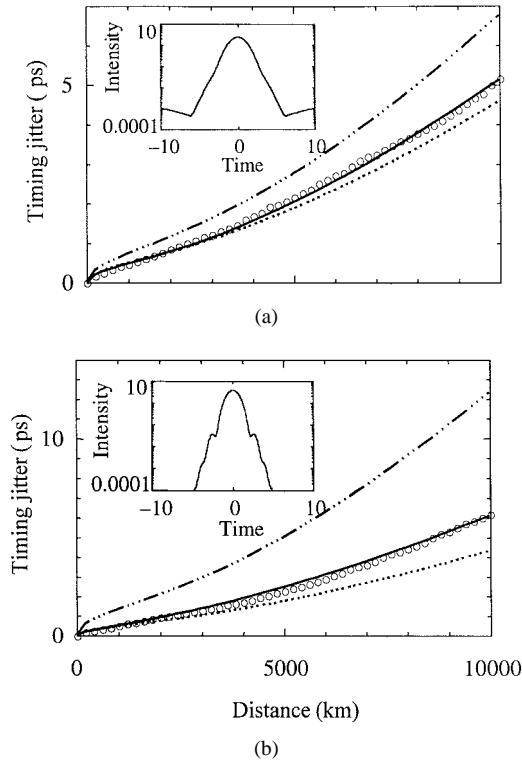
Fig. 1.   The root-mean-square central time of the pulse versus distance for a dispersion-managed soliton system. Inserted graphs are intensity profiles of the dispersion-managed solitons plotted on a logarithmic scale. Circles are results of Monte Carlo simulations, solid lines are results of our theory, and the broken lines and dots represent the Gordon–Haus theory and reduced Gordon–Haus theory, respectively; $t_{\rm FWHM} = 20$ ps, losses are 0.21 db/km; (a) dispersion coefficients are $\beta_1'' = -3.0$ ps^2/km and $\beta_2'' = 2.8$ ps^2/km, theamplifier distance is 50 km, amplifiers are placed at the edges and at the midpoints of normaland anomalous dispersion spans, span lengths are $L_1 = L_2 = 100$ km, peak power at the midpoint of the anomalous dispersion span is 4.12 mW and (b) dispersion coefficients are $\beta_1'' = -3.75$ ps^2/km and $\beta_2'' = 3.55$ ps^2/km, amplifiers are placed at the edges of the spans, amplifier distance is 100 km, span lengths are $L_1 = L_2 = 100$ km, peak power at the midpoint of the anomalous span is 1.39 mW. Here, β_j'' is the dispersion coefficient and L_j is the length of span j.

even with the standard reduction factor, does not take into account the dependence of the jitter on the pulse profile, as it is based on a hyperbolic-secant pulse shape. That is why the deviation from the reduced Gordon–Haus formula becomes considerable in the case of Fig. 1(b). On the other hand, there is excellent agreement with our theory. For strong dispersion management, dispersion-managed solitons can exist with zero and normal path average dispersion [13]. Our calculations show that despite the complete dispersion compensation there is a residual timing jitter for zero average dispersion. In this case, however, the frequency jitter term A no longer makes the largest contribution to the timing jitter.

Fig. 2 shows dependence of the timing jitter on distance and the different contributions of the A, B, and C terms for zero average dispersion. We note that, as follows from (10), A and C are always positive. However, for this configuration the B term is larger then either A and B and negative, which means that the chirp-induced central time shift significantly suppresses the timing jitter caused by the frequency shift and time offset. We note that the inner integral for B in (10) is proportional to the chirp α due to (13). Hence, amplifiers
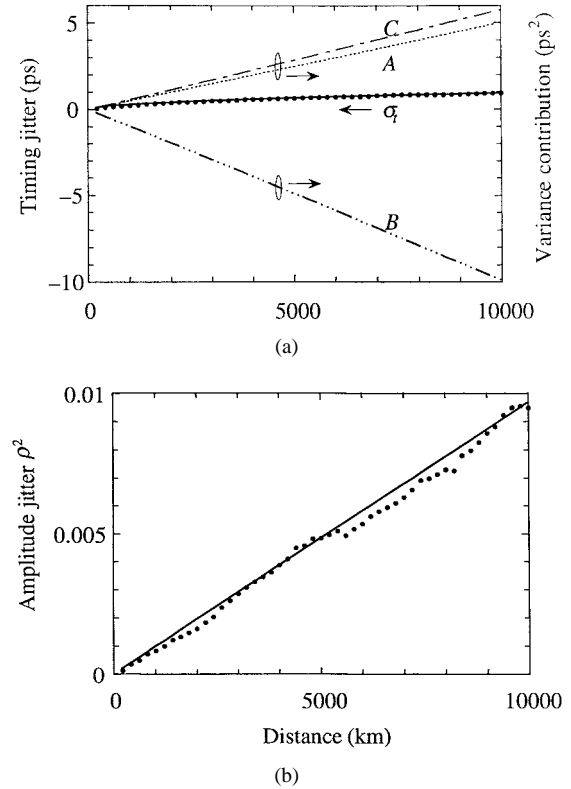

Fig. 2.   (a) Timing jitter σ_t and (b) amplitude jitter ρ versus distance for a dispersion-managed soliton at zero average dispersion. In (a), we also show the individual contribution of the terms A, B, and C. Solid lines are results of the theory, dots are results of Monte Carlo simulations; the peak power at the midpoint of the anomalous dispersion span is 4.33 mW and $t_{\rm FWHM} = 20$ ps, $\beta_1'' = -\beta_2'' = -11$ ps^2/km, $L_1 = L_2 = 100$ km. Amplifiers are placed atthe edges and at the midpoints of the spans every 50 km.

located at the midpoints make a small contribution to B because the chirp at the midpoint is small. However, amplifiers located at the ends of the spans always yield a negative contribution to B. Thus, locating the amplifiers at the ends of the spans reduces the timing jitter. The resultant timing jitter agrees perfectly with the Monte Carlo simulations.

Fig. 2(b) shows the amplitude jitter, i.e., the normalized variance of the photon number in the pulse, versus distance. It grows linearly and remains well below 0.028 up to 10 Mm. From [8], we infer that $\rho^2 = 0.028$ corresponds to a bit error rate of 10^{-9}. Fig. 3 illustrates the results for two different arrangements of the amplifiers. In the first, the amplifiers are placed at the edges of the spans, and, in the second, the amplifiers are placed at the midpoints. The peak power and the pulse duration at the midpoint of the anomalous span are 1.2 mW and 20 ps respectively. Since the chirp is small at the midpoints, the B term is small in Fig. 3(b) in contrast to Fig. 3(a). The resultant timing jitter is larger in Fig. 3(b) then in Fig. 3(a), because the B term does not partially cancel out the A and C terms.

Finally, we compared our linearization approach to Monte Carlo simulations for the configuration reported in the recent experiment of Carter and Jacob [14] on ultra-long-distance propagation of dispersion-managed solitons in a filtered recirculating fiber loop consisting of 100 km of fiber in the normal dispersion regime and about 7 km of fiber in the anomalous
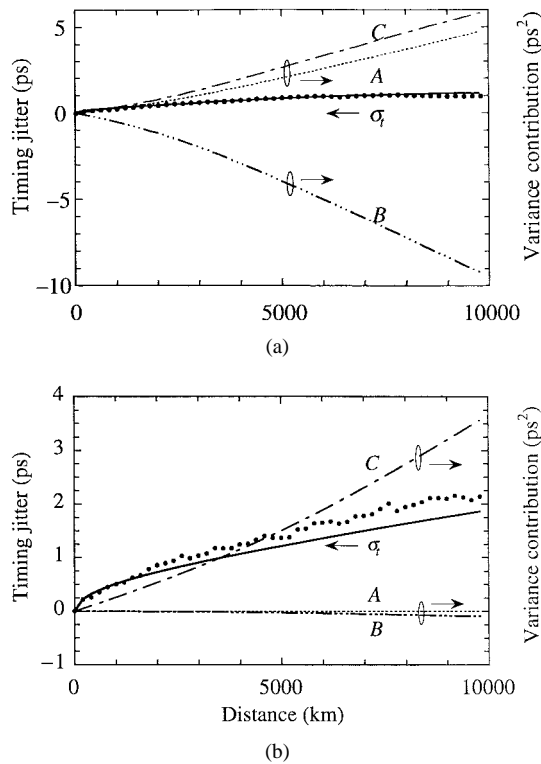
(a)

(b)

Fig. 3. Dependence of the timing jitter σ_t and the contributions of the terms A, B, and C to the central time variance on distance for the dispersion-managed soliton at zero average dispersion in a system with $L_1 = L_2 = 50$ km, peak power in the midpoint of the anomalous dispersion span of 1.21 mW, amplifier spacing of 50 km and other parameters being the same as in Fig. 2 for the amplifier arrangements at (a) the edges and at (b) the midpoints of the spans.

dispersion regime. Fig. 4 shows the timing jitter in the loop as a function of propagation distance. The pulse durations in the midpoints of the anomalous and normal dispersion spans were 9.5 ps and 12.5 ps respectively. The solid curve in Fig. 4 was calculated based on (22) and (23), the black circles show the result of Monte Carlo simulations with 200 realizations of the ASE noise, and the open circles show the experimental results. We note that the timing jitter grows more slowly than in the un-filtered case of Fig. 1. We find a remarkable agreement of our approach with the Monte Carlo simulations and with the experimental data over the entire propagation distance of 22 Mm.

B. RZ Pulses

We simulated propagation of RZ signals by launching raised-cosine prechirped pulses of the form $u(0, t) = A[1 - \cos(t/t_0)]\exp(-it^2/t_c^2)$ with $t_0 = 32$ ps, $t_c^2 = 1000$ ps^2, and a peak power of 1.08 mW at the beginning of the anomalous dispersion span. We studied two neighboring pulses, with periodic boundary conditions, which allowed us to include the effect of interpulse interference. In our Monte Carlo simulation, we calculated the timing jitter and amplitude jitter using the later pulse. Fig. 5 shows the dependence of the timing and amplitude jitter on distance. We show the RZ pulse evolution in the presence of noise in Fig. 6. The dynamics of the timing jitter is close to that of Fig. 2 for the dispersion-managed soliton, although the final jitter is a little larger.
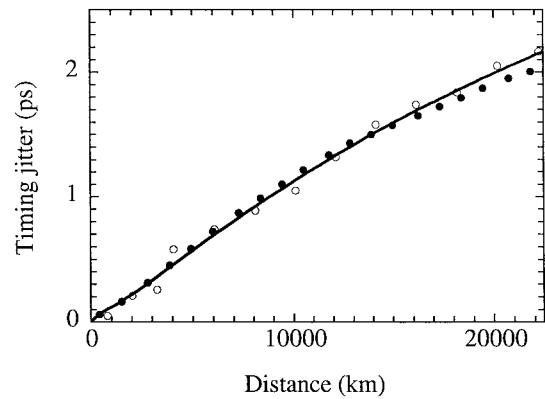

Fig. 4. Comparison of the timing jitter calculated using the linearization approach (solid line) with Monte Carlo simulations (black circles) to the experiment of Carterand Jacob[14] on ultralong-distance propagation of the dispersion-managed solitons in a recirculating fiber loop with an average dispersion of 0.04 ps/nm-km. The experimental results are plotted as open circles.
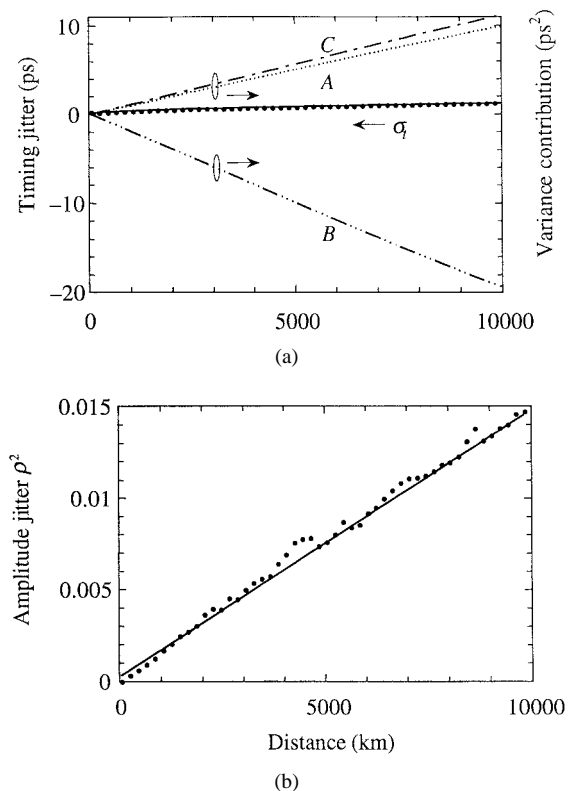

(a)

(b)

Fig. 5. Plots of the (a) timing jitter σ_t and (b) amplitude jitter ρ^2 versus distance for an RZ pulse at zero average dispersion. Fig. 5(a) shows individual contributions of the A, B, and C terms to the pulse position variance versus distance. Solid lines are results of the theory; dots are the results of the Monte Carlo simulations; pulse duration and peak power at the midpoint of the anomalous dispersion span are $t_{\mathrm{FWHM}} = 20$ ps and 1.08 mW, $\beta_1'' = -\beta_2'' = -11$ ps^2/km, $L_1 = L_2 = 100$ km. Amplifiers are placed atthe edges and at the midpoints of the spans every 50 km.

As in the previous cases there is a good agreement between the linearization approach and Monte Carlo simulations. In this case, timing jitter remains small and the major source of errors is the amplitude jitter. There is some drift of the amplitude jitter at large distances which may indicate that the linearization approach is breaking down.
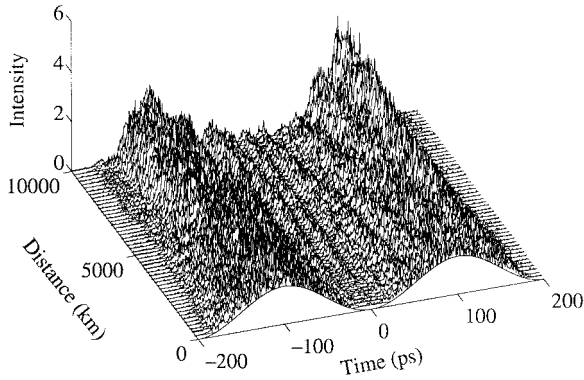
Fig. 6. Evolution of the RZ pulse in the presence of noise for the system in Fig. 5.

C. NRZ Pulses

There are significant pattern dependences in the nonlinear pulse evolution of the marks ("1's") in the NRZ format due to intersymbol interference. Thus, we must explore different combinations of the marks and spaces ("0's"). Anderson and Lyle [15] have shown that in many cases, the behavior is dominated by the eight combinations: 0-0-0, 0-0-1, 0-1-0, 0-1-1, 1-0-0, 1-0-1, 1-1-0, and 1-1-1. Thus, in our study of amplitude and timing jitter, it is appropriate for us to focus on the strings 0-1-0, 0-1-1-0, and 0-1-1-1-0. We simulated propagation of these signals by launching ideal rectangular pulses with a power of 0.35 mW using the same dispersion map and amplifier arrangement as in Fig. 2. The time duration is 100 ps per bit, corresponding to a 10 Gb/s bit rate. While real NRZ signals have rounded edges, the use of rectangular pulses provides a more stringent test of our approach. The results are shown in Figs. 7–12. The frequency jitter given by the A term is significantly larger for the pattern 0-1-0 than for the patterns 0-1-1-0 and 0-1-1-1-0 because the bandwidth is largest and the energy is smallest in this case. Similarly, the B and C terms decrease in magnitude as we move from the pattern 0-1-0 to the pattern 0-1-1-0 to the pattern 0-1-1-1-0. However, the resultant timing jitter is a few picoseconds in all three cases. The amplitude jitter is the largest for the pattern 0-1-0 and decreases for 0-1-1-0 and 0-1-1-1-0. However, this result has been normalized to the total pulse energy. If we examine instead the amplitude jitter per bit, we find that this value is constant as we change the pattern. We find good agreement between the linearization approach and Monte Carlo simulations, although it appears that the linearization approach may be beginning to break down beyond 5000 km.

IV. ESTIMATES OF THE BIT ERROR RATE

Calculation of the timing and amplitude jitter leads to important insights into the physical sources of errors in communication systems. Moreover, these quantities can be measured experimentally, allowing us to compare theory and experiment [14]. However, the bit error rate is more important than either of these quantities for designing systems, and one would ideally like to use these calculations to infer the bit error rate. In principle, that is difficult to do accurately. First, one is typically interested in bit error rates that are 10^{-9}
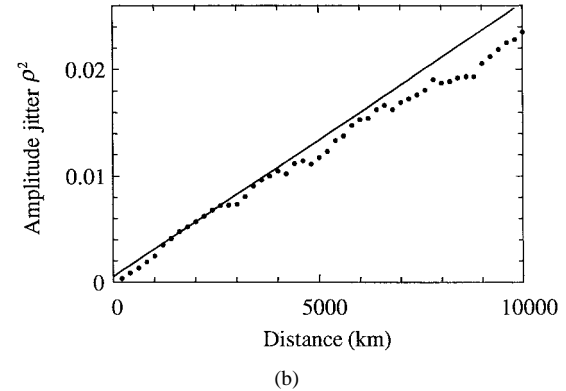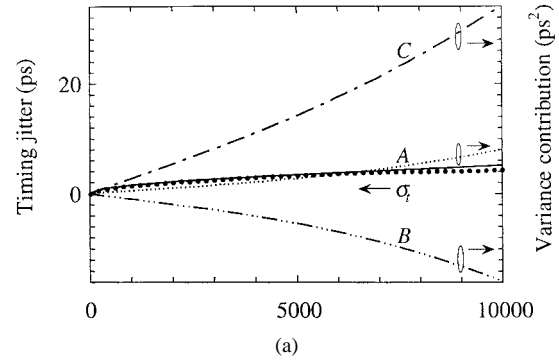

(a)

(b)

Fig. 7. Plots of the (a) timing jitter σ_t and (b) the amplitude jitter ρ versus distance for a 0-1-0 NRZ pulse of 100 ps at zero average dispersion. Fig. 7(a) shows the individual contributions of the terms A, B, and C to the pulse central time variance versus distance. Pulse peak power is 0.35 mW; system parameters are the same that in Fig. 3.
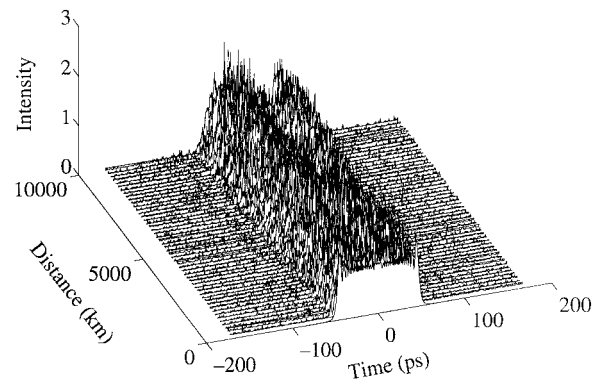

Fig. 8. Evolution of the 0-1-0 NRZ pulse in the presence of noise for the system in Fig. 7.

or even lower, implying that one must accurately know the tails of the distribution functions for the time shifts and the amplitudes. Even when the jitter, which corresponds to the variance of the distribution function is determined accurately using the linearization assumption, the tails may not be [16], [17]. Second, actual bit errors depend critically on the receiver design. Appropriate design of both the optical and electrical filters can play a crucial role in reducing the errors [18].

In this section, we will show how to estimate the bit error rate, using a simple integrate-and-dump receiver. We will assume that spontaneous-spontaneous beat noise is negligible throughout most of this section, although we will briefly consider its effect at the end. Even in this case we cannot
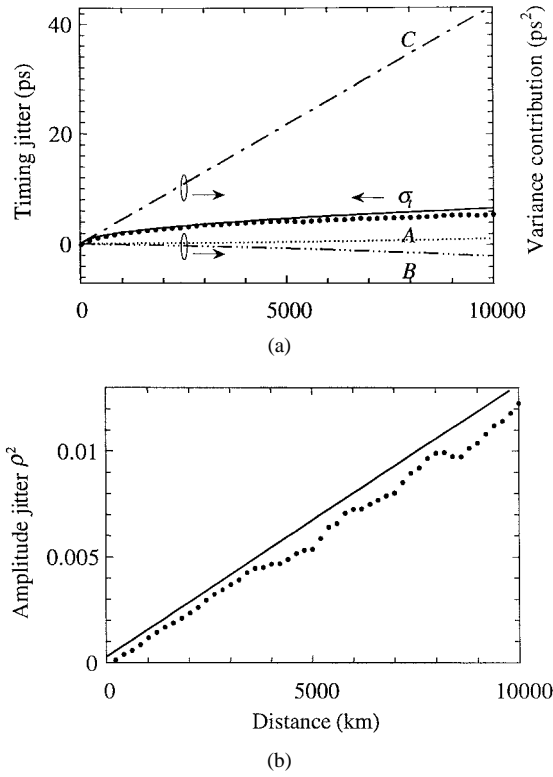
(a)

(b)

Fig. 9. Results for the same system as in Fig. 7, but for a 0-1-1-0 NRZ pulse.

(a)

(b)

Fig. 11. Results for the same system as in Fig. 7, but for a 0-1-1-1-0 NRZ pulse.

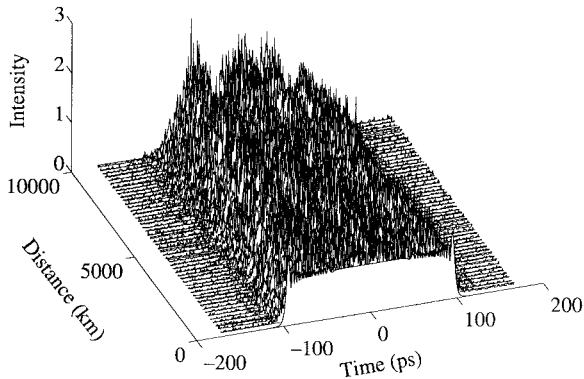Fig. 10. Evolution of the 0-1-1-0 NRZ pulse in the presence of noise for the system in Fig. 9.
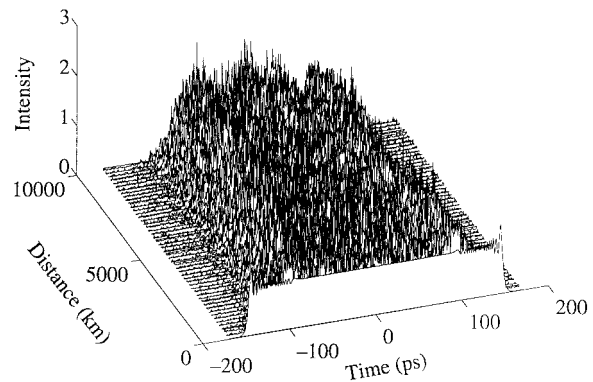
Fig. 12. Evolution of the 0-1-1-1-0 NRZ pulse in the presence of noise for the system in Fig. 11.

completely determine the bit error rate from just the timing and amplitude jitter because the amplitude jitter is typically accompanied by pulse distortion. For example, in the case of standard solitons, the pulse duration is proportional to $U^{1/2}$ [19]. However, it is often the case that either the timing or the amplitude jitter becomes the dominant source of errors. When the timing jitter dominates, then it is possible to calculate the bit error rate due to it while neglecting amplitude jitter and the accompanying pulse distortion. Conversely, when amplitude jitter dominates over timing jitter and the time window is large enough to include the entire pulse, then pulse distortion does not effect the calculation of the bit error rate due to amplitude jitter.

We begin by making a key observation: The Langevin noise source $\hat{F}(z,t)$ can be treated as a Gaussian-distributed white noise source [20] in each point z. The Gaussian noise sources
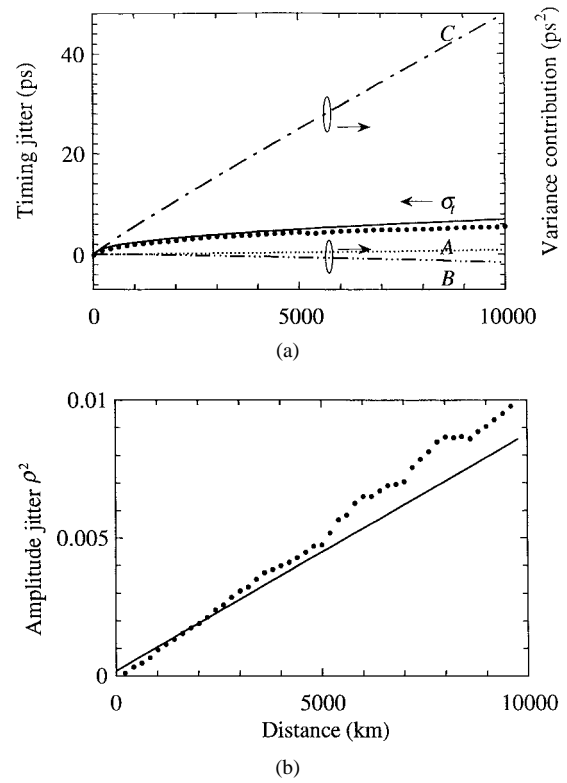
in different points z are statistically independent. Since dt_p/dz and dU/dz are a linear superposition of contributions from $\hat{F}$ and $\hat{F}^*$, as shown in (4) and (25), it follows that t_p and U must be Gaussian-distributed [12]. Thus, we may write their probability distribution functions explicitly as

$$P(t_p) = \frac{1}{\sqrt{2\pi}\sigma_t} \exp\left[-\frac{(t_p - \langle t_p \rangle)^2}{2\sigma_t^2}\right], \qquad (30)$$

$$W(U) = \frac{1}{\sqrt{2\pi}\sigma_U} \exp\left[-\frac{(U - \langle U \rangle)^2}{2\sigma_U^2}\right] \qquad (31)$$

where we recall that $\langle t_p \rangle$ and $\langle U \rangle$ are respectively the central time and photon number in the absence of noise.

Errors occur when the energy of a mark inside the time window falls below a threshold U_{th} which is determined

by the background optical noise in the spaces and electrical noise in the receiver. We will designate the timing window $-T_w/2 < t - \langle t_p \rangle < T_w/2$. Since receivers use clock recovery to locate the timing window, the window will be centered about the overall average $t = \langle t_p \rangle$. The number of photons in the timing window may be written

$$
\begin{aligned}
U_w(t_p - \langle t_p \rangle) &= \int_{\langle t_p \rangle - T_w/2}^{\langle t_p \rangle + T_w/2} |\bar{u}(t - t_p)|^2 \, dt \\
&= \int_{-T_w/2}^{T_w/2} |\bar{u}(t' - t_p - \langle t_p \rangle)|^2 \, dt'.
\end{aligned}
\quad (32)
$$

There is some value of $|t_p - \langle t_p \rangle|$ beyond $U_w(t_p - \langle t_p \rangle) < U_{\text{th}}$. We will designate this value as $t_{p,\text{th}} - \langle t_p \rangle$. Then, the bit error rate is given by

$$
\begin{aligned}
&\text{Prob}[U_w(t_p - \langle t_p \rangle) < U_{\text{th}}] \\
&= 2 \int_{t_{p,\text{th}} - \langle t_p \rangle}^{\infty} \frac{1}{\sqrt{2\pi}\sigma_t} \exp\left(-t^2/2\sigma_t^2\right) dt \\
&= \text{erfc}\left(\frac{t_{p,\text{th}} - \langle t_p \rangle}{\sqrt{2}\sigma_t}\right).
\end{aligned}
\quad (33)
$$

The factor of two preceding the integral in (33) accounts for the two-sided nature of the distribution, i.e., errors occur both when $t_p - \langle t_p \rangle > t_{p,\text{th}} - \langle t_p \rangle$ and when $t_p - \langle t_p \rangle < -(t_{p,\text{th}} - \langle t_p \rangle)$. While the specific shape of the final pulse plays an important role in determining the dependence of $t_{p,\text{th}}$ on U_{th}, the bit error rate is given by (33) regardless of the shape given that σ_t is fixed. This is a consequence of (30).

We may now calculate the bit error rate due to amplitude jitter, and we find

$$
\begin{aligned}
\text{Prob}(U < U_{\text{th}}) &= \int_0^{U_{\text{th}}} \frac{1}{\sqrt{2\pi}\sigma_U} \exp\left[-\frac{(U - \langle U \rangle)^2}{2\sigma_U^2}\right] dU \\
&= \frac{1}{2}\text{erfc}\left(\frac{\langle U \rangle - U_{\text{th}}}{\sqrt{2}\sigma_U}\right)
\end{aligned}
\quad (34)
$$

which again has a very simple form. In obtaining (34), we set $\langle U \rangle / \sigma_U \to \infty$. Since the energy cannot be negative, it is physically meaningless that the probability distribution function given by (31) allows negative energies. This result is a consequence of neglecting the spontaneous-spontaneous beat noise and will not affect (34) as long as it is genuinely negligible at the threshold value U_{th}. However, when there are many noise modes, then the spontaneous-spontaneous beat noise may make a significant contribution to the total energy even though the contribution of a single mode is negligibly small. Marcuse [8] included this noise, assuming that the noise energy was equally divided among all the noise modes. The number M of the complex modes is given by $M = B_{\text{opt}}T_w$, where B_{opt} is the optical bandwidth. Thus, if for example, we consider a system in which a single optical wavelength channel occupies a bandwidth of 100 GHz and the receiver window is 100 ps, then there are 10 complex modes. In this case, the number of photons per mode U_{mode} is given by

$$
U_{\text{mode}} = n_{\text{sp}}(G - 1)K \quad (35)
$$

where G is the amplifier gain and K is the number of in-line amplifiers just like in (28). One then finds that the probability distribution function for the energy in a space $P_0(U)$ is given by [8]

$$
P_0(U) = \frac{1}{(M-1)!} \frac{U^{M-1}}{U_{\text{mode}}^M} \exp\left(-\frac{U}{U_{\text{mode}}}\right) \quad (36)
$$

while the probability distribution for the energy in a mark is given by [8]

$$
\begin{aligned}
P_1(U) &= \frac{1}{U_{\text{mode}}} \left(\frac{U}{\langle U \rangle}\right)^{(M-1)/2} \exp\left(-\frac{U + \langle U \rangle}{U_{\text{mode}}}\right) \\
&\times I_{M-1}\left(2\frac{\sqrt{U\langle U \rangle}}{U_{\text{mode}}}\right)
\end{aligned}
\quad (37)
$$

where I_{M-1} is the modified Bessel function of order $M - 1$. Marcuse [8] has discussed in some detail the consequence of replacing (37) with (31). For the RZ and NRZ systems that we studied in Section III, it is possible to estimate that the error made in determining the threshold value at which the error rate reaches 10^{-9} is about 10–20%, assuming $M = 10$. A more refined estimate is not possible for the systems that we considered because a set of modes that is originally orthogonal is mixed together by the nonlinearity so that they do not remain orthogonal. Physically, the signal can parametrically pump some noise modes due to the four-wave mixing (FWM). Thus, the assumption that the noise energy is equally divided among the modes in the case when spontaneous–spontaneous beat noise becomes significant is suspect at best, particularly in real systems with more complicated receiver filters than we have considered. In systems with inline filters, as is the case in many soliton systems [14], this assumption is clearly false. A careful investigation of this issue remains an important open topic for future work.

V. CONCLUSION

In conclusion, we have developed an approach, based on linearizing the modified nonlinear Schrödinger equation (1) around a numerically determined noise-free solution. This approach allows us to determine the timing jitter and the amplitude jitter for arbitrary pulse shapes. Its principal advantage is that it allows us to avoid numerically time-consuming Monte Carlo simulations. We have applied this approach to DMS, RZ, and NRZ pulse formats, and we have validated it by comparison to Monte Carlo simulations. We have shown that within the limits of validity of the linearization approximation, the timing jitter is Gaussian-distributed. When, in addition, spontaneous-spontaneous beat noise may be neglected, the energy is also Gaussian-distributed. We have used this result to separately estimate the bit error rate due to timing jitter and amplitude jitter when one or other is the dominant source of errors.

REFERENCES

[1] J. P. Gordon and H. A. Haus, "Random walk of coherently amplified solitons in optical fiber transmission," *Opt. Lett.*, vol. 11, pp. 665–667, 1986.

[2] H. A. Haus, "Quantum noise in solitonlike repeater system," *J. Opt. Soc. Amer. B*, vol. 8, pp. 1122–1126, 1991.

[3] N. J. Smith, W. Forysiak, and N. J. Doran, "Reduced Gordon-Haus jitter due to enhanced power solitons in strongly dispersion managed systems," *Electron. Lett.*, vol. 32, pp. 2085–2086, 1996.

[4] G. M. Carter, J. M. Jacob, C. R. Menyuk, E. A. Golovchenko, and A. N. Pilipetskii, "Timing-jitter reduction for a dispersion-managed soliton system: Experimental evidence," *Opt. Lett.*, vol. 22, pp. 513–515, 1997.

[5] S. K. Turitsyn, "Theory of average pulse propagation in high-bit-rate optical transmission systems with strong dispersion," *JETP Lett.*, vol. 65, pp. 845–850, 1997.

[6] S. Kumar and A. Hasegawa, "Quasisoliton propagation in dispersion-managed optical fibers," *Opt. Lett.*, vol. 22, pp. 372–375, 1997.

[7] T. Georges, F. Favre, and D. L. Guen, "Theoretical and experimental study of soliton transmission in dispersion managed links," *Inst. Electron. Inf. Commun. Eng. Trans. Electron.*, vol. E81-C, pp. 226–231, 1998.

[8] D. Marcuse, "Derivation of analytical expressions for the bit-error probability in lightwave systems with optical amplifiers," *J. Lightwave Technol.*, vol. 8, pp. 1816–1823, 1990.

[9] P. A. Humblet and M. Azizoglu, "On the bit error rate of lightwave systems with optical amplifiers," *J. Lightwave Technol.*, vol. 9, pp. 1576–1082, 1991.

[10] A. Mecozzi, "Long-distance transmission at zero dispersion; combined effect of the Kerr nonlinearity and the noise of the in-line amplifiers," *J. Opt. Soc. Amer. B*, vol. 12, pp. 462–469, 1994.

[11] R. Hui, M. O'Sullivan, A. Robinson, and M. Taylor, "Modulation instability and its impact in multispan optical amplified IMDD systems: Theory and experiments," *J. Lightwave Technol.*, vol. 15, pp. 1071–1082, 1997.

[12] J. G. Proakis, *Digital Communications*. New York: McGraw-Hill, ch. 2, pp. 17–81, 1995. (See especially Sec. 2.14.)

[13] J. H. B. Nijhof, N. J. Doran, W. Forysiak, and F. M. Knox, "Stable soliton-like propagation in dispersion managed systems with net anomalous, zero and normal dispersion," *Electron. Lett.*, vol. 33, pp. 1726–1727, 1997; see also, V. S. Grigoryan and C. R. Menyuk, "Dispersion-managed solitons at normal average dispersion," *Opt. Lett.*, vol. 23, pp. 609–611, 1998; see also, S. K. Turitsyn and E. G. Shapiro, "Dispersion-managed solitons in optical amplifier transmission systems with zero average dispersion," *Opt. Lett.*, vol. 23, pp. 682–684, 1998; see also, J. N. Kutz and S. G. Evangelides Jr., "Dispersion-managed breathers with average normal dispersion," *Opt. Lett.*, vol. 23, pp. 685–687, 1998; A. Berntson, N. J. Doran, W. Forysiak, and J. H. B. Nijhof, "Power dependence of dispersion-managed solitons for anomalous, zero, and normal path-average dispersion," *Opt. Lett.*, vol. 23, pp. 900–902, 1998; see also, Y. Chen and H. A. Haus, "Dispersion-managed solitons with net positive dispersion," *Opt. Lett.*, vol. 23, pp. 1013–1015, 1998; see also, T. I. Lakoba, J. Yung, D. J. Kaup, and B. A. Malomed, "Conditions for stationary pulse propagation in the strong dispersion management regime," *Opt. Commun.*, vol. 149, pp. 366–375, 1998.

[14] G. M. Carter and J. M. Jacob, "Dynamics of solitons in filtered dispersion-managed system," *IEEE Photon. Technol. Lett.*, vol. 10, pp. 546–548, 1998.

[15] C. J. Anderson and J. A. Lyle, "Technique for evaluating system performance using Q in numerical simulations exhibiting intersymbol interference," *Electron. Lett.*, vol. 30, pp. 71–72, 1994.

[16] C. R. Menyuk, "Non-Gaussian corrections to the Gordon-Haus distribution resulting from soliton interactions," *Opt. Lett.*, vol. 20, pp. 285–288, 1995.

[17] T. Georges, "Bit error rate degradation of interacting solitons owing to non-Gaussian statistics," *Electron. Lett.*, vol. 31, pp. 1174–1175, 1995; T. Georges, "Study of non-Gaussian timing jitter statistics induced by soliton interaction and filtering," *Opt. Commun.*, vol. 123, pp. 617–623, 1996.

[18] K. Ogawa, L. D. Tzeng, Y. K. Park, and E. Sano, "Advances in high bit-rate transmission systems," in *Optical Fiber Telecommunications IIIA*, I. P. Kaminow and T. L. Koch, Eds., San Diego, CA: Academic, 1997, ch. 11, pp. 336–372.

[19] A. Hasegawa and Y. Kodama, *Solitons in Optical Fiber Communications*. Oxford, U.K.: Clarendon, 1995, ch. 3.1, pp. 17–28.

[20] R. Loudon, *The Quantum Theory of Light*. Oxford, U.K.: Clarendon, 1983, ch. 6, pp. 211–250.

V. S. Grigoryan, photograph and biography not available at the time of publication.

C. R. Menyuk, photograph and biography not available at the time of publication.

R.-M. Mu, photograph and biography not available at the time of publication.